Electronic Supplementary Information

Experimental section

Materials: Zinc nitrate hexahydrate ($Zn(NO_3)_2 \cdot 6H_2O$), ammonium fluoride (NH_4F), urea (CH_4N_2O), cobalt nitrate hexahydrate ($Co(NO_3)_2 \cdot 6H_2O$), thiourea (CH_4N_2S), hydrochloric acid (HCl), and ethanol (C_2H_5OH) were purchased from Aladdin Reagent Inc. Nickel foam was purchased from Shenzhen Neware Electronics Co. Ltd. The ultrapure water used in the whole experiments was purified by a Millipore system. All related chemicals in the experiments can be used without further purification.

Synthesis of the ZnO nanoflake arrays (NFAs) on nickel foam substrate: The nickel foam with a diameter of 14 mm was ultrasonically cleaned by 3 M HCl, ethanol and deionized water respectively, aiming to remove impurities and oxides on the surface. The ZnO NFAs on nickel foam was synthesized by a hydrothermal method. Typically, 4 mmol of zinc nitrate hexahydrate, 8 mmol of ammonium fluoride, and 10 mmol of urea were dissolved in 80 mL of deionized water and vigorously stirred for 30 min to form a homogeneous mixed solution. Then, the as-prepared solution was transferred to a 100 ml Teflon-lined autoclave and the cleaned nickel foam was horizontally transferred to the bottom of the autoclave. After that, the autoclave was sealed and kept in an oven at 120 °C for 8 h. After the hydrothermal reaction was completed, the Zn hydroxide on the nickel foam was washed several times with ethanol and deionized water and vacuum dried overnight at 70 °C. Finally, Zn hydroxide was heated in the air at 600 °C for 3 h to obtain ZnO NFAs. The mass

loading of ZnO NFAs on each nickel foam after annealing was about 2 mg cm^{-2}.

Electrodeposition of CoS nano-films (NFs) on ZnO NFAs: The CoS NFs electrodeposited on ZnO NFAs were implemented on a CHI660E electrochemical workstation. The ZnO NFAs on the nickel foam acted as the working electrode for electrodeposition of the CoS layer. In addition, Pt wire, saturated calomel electrode, and 100 mL of deionized water containing 10 mmol of cobalt nitrate hexahydrate and 70 mmol of thiourea were used as the counter electrode, reference electrode and electrolyte, respectively. The electrodeposition process was performed by using CV technique at a scan rate of 5 mV s^{-1} in a voltage range of −1.2 to 0 V for 10 cycles. The obtained ZnO NFAs/CoS NFs electrode was rinsed several times with deionized water and then dried in vacuum at 50 °C for 6 h. The mass loading of CoS NFs on each nickel foam after electrodeposition was about 0.5 mg cm^{-2}. For comparison, CoS nano-films were directly electrodeposited on the cleaned nickel foam (denoted as CoS NFs). In addition, the ZnO NFAs/CoS NFs-5 (mass loading of CoS NFs: about 0.25 mg cm^{-2}) and ZnO NFAs/CoS NFs-20 (mass loading of CoS NFs: about 1.0 mg cm^{-2}) were obtained using the same electrodeposition process by changing the number of CV cycles to 5 and 20, respectively.

Materials characterization: X-ray powder diffraction (XRD) patterns were measured using a D/Max-III diffractometer (Rigaku Co., Japan) with a Cu Kα radiation. X-ray photoelectron spectroscopy (XPS) was performed using an Escalab 250Xi instrument with a monochromatic Al Kα radiation source. The morphologies of the samples were characterized by a JSM-7600F field-emission scanning electron

microscope (FESEM, Hitachi Co., Japan) at an operating voltage of 5.0 kV. The TEM images and high-resolution TEM images were obtained by a Tecnai G^2 F20 S-Twin TMP transmission electron microscope (TEM, FEI Co., USA) and the instrument was equipped with an X-ray energy-dispersive spectrometer (EDS) to analyze the element contents of the samples.

Electrochemical measurements: Electrochemical tests were performed on a CHI660E electrochemical workstation. The electrochemical properties were obtained in a three-electrode system including working electrode (ZnO NFAs/CoS NFs, ZnO NFAs, CoS NFs), counter electrode (Pt wire), reference electrode (saturated calomel electrode) and electrolyte (2 M KOH solution). Cyclic voltammetry (CV) and galvanostatic charge and discharge tests were carried out in a three-electrode system to evaluate the electrochemical properties of the samples. Electrochemical impedance spectroscopy (EIS) was measured in the frequency range of 100 kHz to 0.01 Hz with the amplitude of 5 mV. The specific capacitances of these electrode materials were based on the discharge time at different current densities in the GCD curves calculated by using the following equation.[1-3]

$$C_s = \frac{I \times \Delta t}{m \times \Delta V} \qquad (1)$$

where C_s (F g^{-1}) is the specific capacitance, I (A) is the discharge current, Δt (s) is the discharge time, m (g) is the mass of the active material, and ΔV (V) is the voltage range.

Theoretical Calculation： Theory calculations were performed using Density Functional Theory (DFT) by the CASTEP program in Materials Studio package. The

pseudopotential used in the theoretical calculation was OTFG ultrasoft. The generalized gradient approximation (GGA) with the Perdew-Burke-Ernzerho (PBE) exchange correlation functional was used to treat all electronic energy of 110 exchange correlation. The plane wave basis set cut-off energy is 381 eV. The convergence criteria for the total energy calculation and geometric optimization step were set as below: a self-consistent field (SCF) energy tolerance of 10^{-5} eV·atom^{-1}, a maximum force tolerance of 10^{-1} eV·A^{-1} and a maximum displacement tolerance of 5 × 10^{-3} A.

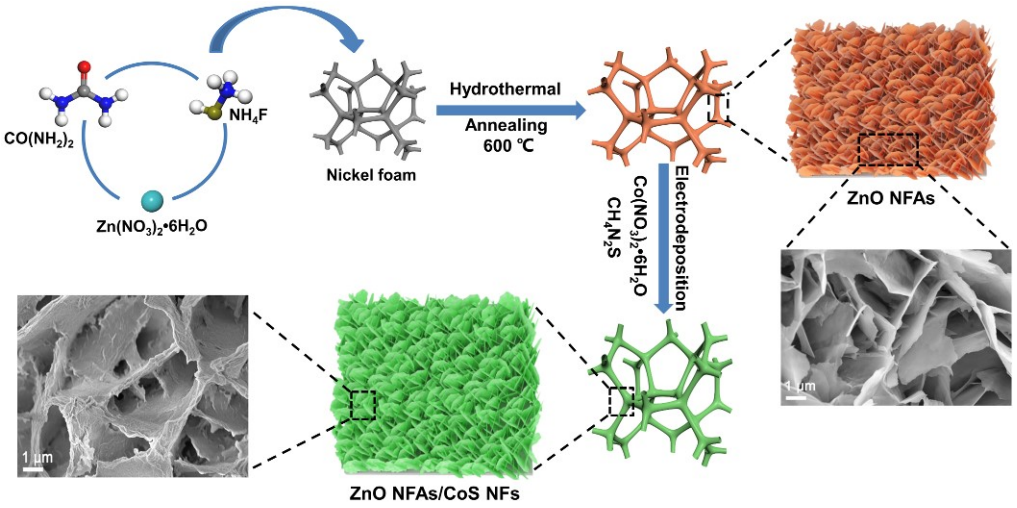

Fig. S1. Schematic illustration of the preparation process of ZnO NFAs/CoS NFs heterostructure on nickel foam.

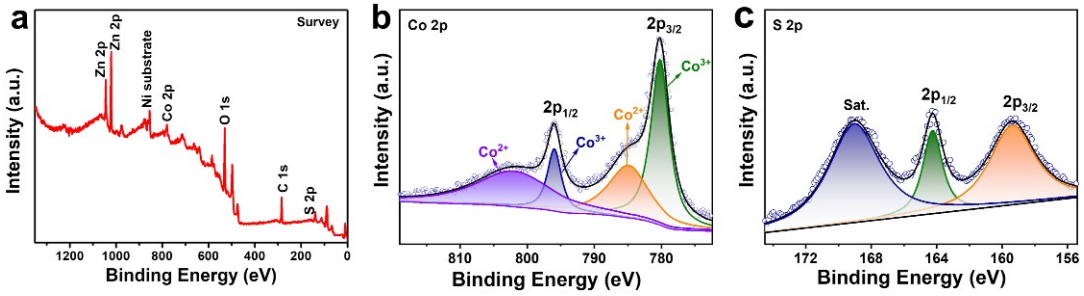

Fig. S2. XPS spectra of ZnO NFAs/CoS NFs for (a) survey spectrum, (b) Co 2p and (c) S 2p.

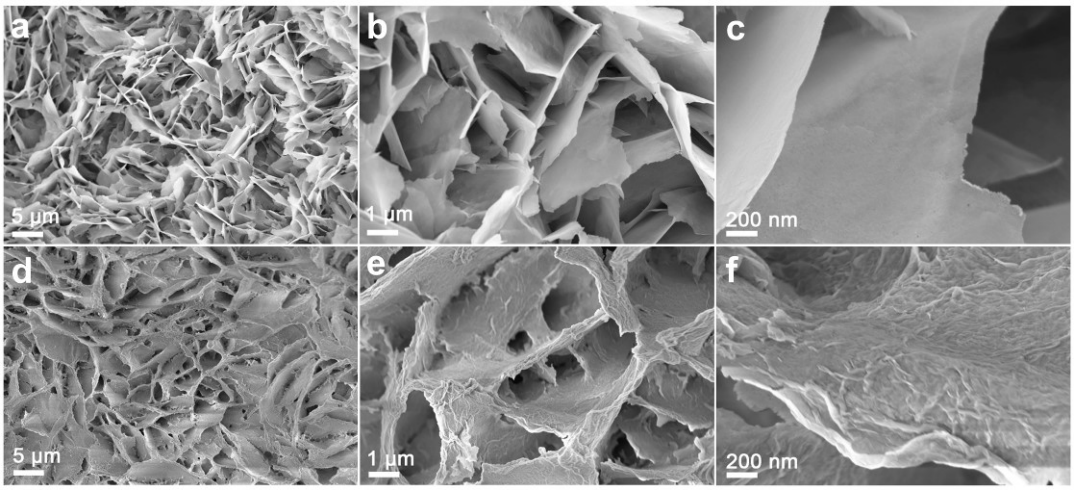

Fig. S3. SEM images of (a-c) ZnO NFAs and (d-f) ZnO NFAs/CoS NFs at different magnifications.

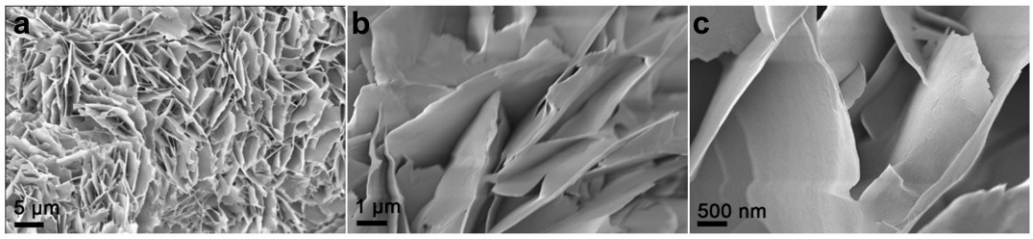

Fig. S4. SEM images of (a-c) Zn layered hydroxide at different magnification.

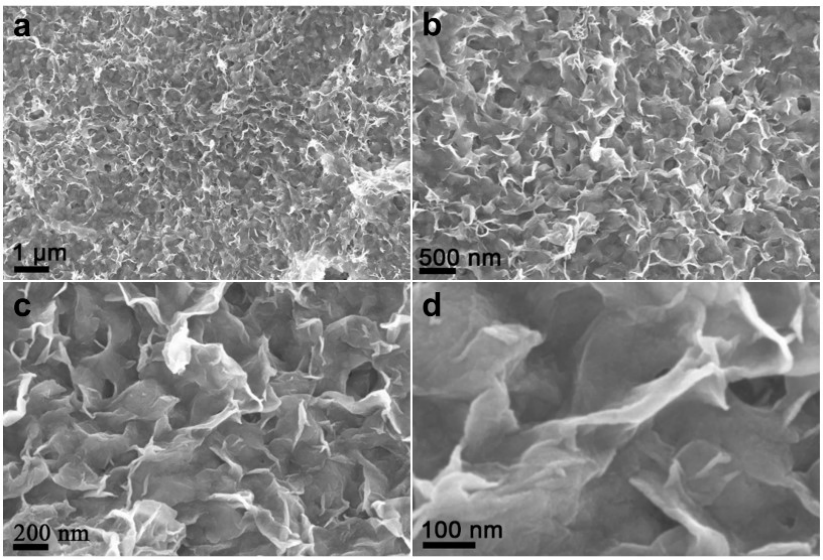

Fig. S5. SEM images of (a-d) CoS NFs at different magnification.

Fig. S3 presents the SEM images of the ZnO NFAs and ZnO NFAs/CoS NFs on the nickel foam. As shown in Fig. S3a and b, the vertical growth of ZnO nanosheet arrays can be clearly observed on the surface of nickel foam. As shown in the high-magnification SEM image (Fig. S3c), a single ZnO nanosheet with thickness of ～20 nm shows smooth surface without evident porous structure. After electrodeposition, as shown in Fig. S3d-f, it is obvious that the three-dimensional crumpled CoS homogeneously coated on the surface of the ZnO nanoflakes, suggesting the successful formation of the heterostructure. This unique hierarchical and highly porous heterostructure provide large specific surface area, which enhances the contact between the electrode and the electrolyte, facilitating ion diffusion and electrolyte penetration into the active material. Additionally, the morphology of ZnO nanoflake arrays remained unchanged after the growth of CoS, suggesting the robust two-dimensional structure not affected by the electrodeposition process. Such a high

structural stability could be originated from the parental Zn layered hydroxide precursor, which demonstrated identical morphology as the oxide obtained after calcination (Fig. S4a-c). The SEM images of the CoS NFs control sample (Fig. S5a-d) clearly show the presence of the wrinkled and porous CoS over the entire surface of the nickel foam.

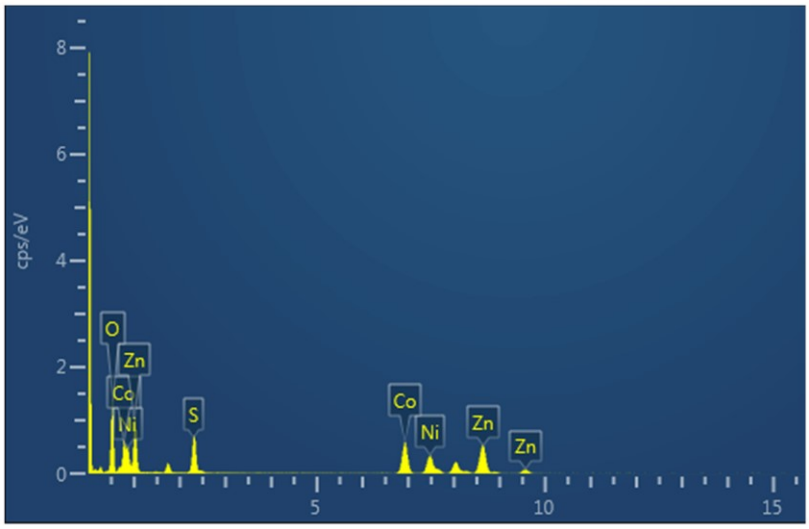

Fig. S6. EDS spectrum of the ZnO NFAs/CoS NFs composite.

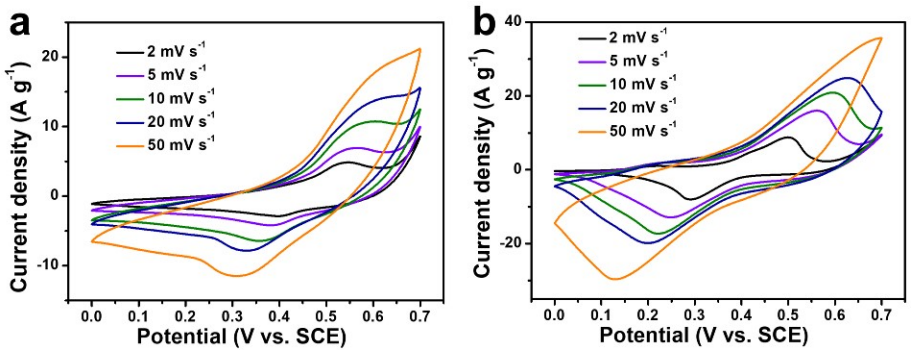

Fig. S7. CV curves of (a) ZnO NFAs and (b) CoS NFs electrodes at different scan rates.

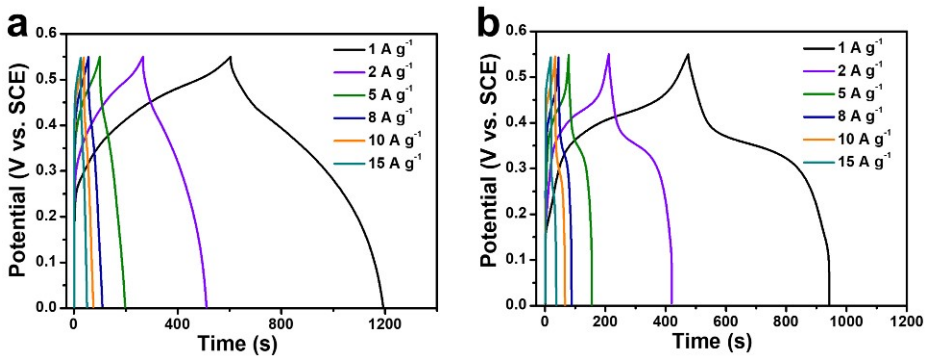

Fig. S8. GCD curves of (a) ZnO NFAs and (b) CoS NFs electrodes at different current densities.

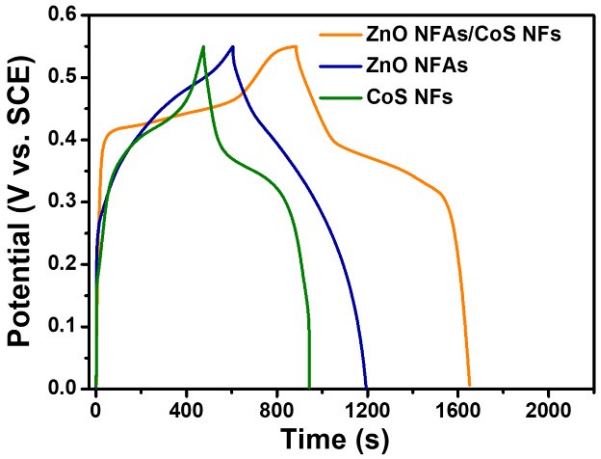

Fig. S9. GCD curves of ZnO NFAs/CoS NFs, ZnO NFAs, and CoS NFs electrodes at a current density of 1 A g^{-1}.

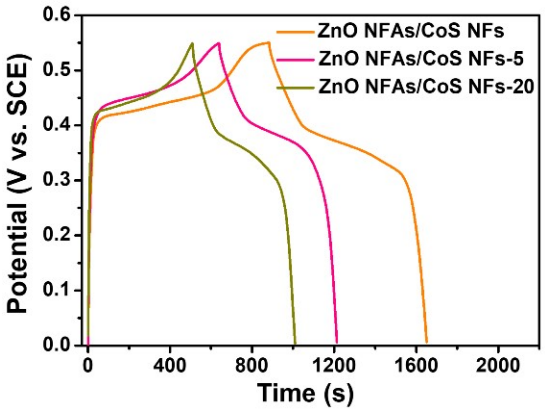

Fig. S10. GCD curves of ZnO NFAs/CoS NFs, ZnO NFAs/CoS NFs-5, and ZnO NFAs/CoS NFs-20 electrodes at a current density of 1 A g^{-1}.

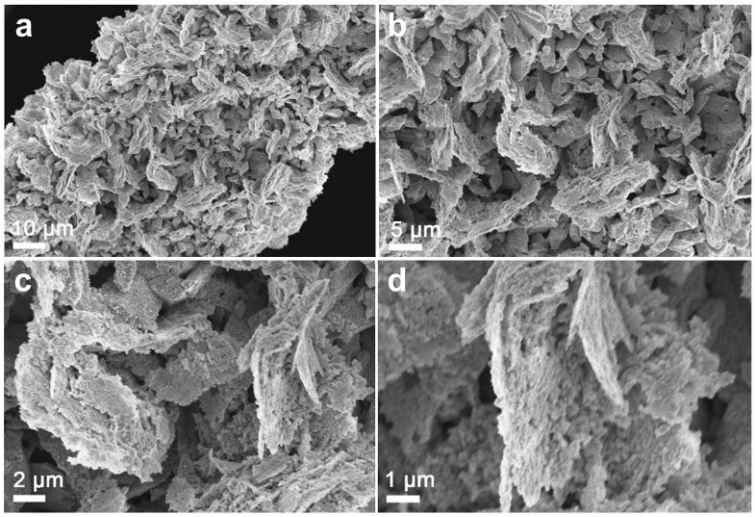

Fig. S11. SEM images of ZnO NFAs/CoS NFs electrode after 5000 cycles.

Table S1 The element content distribution of ZnO NFAs/CoS NFs sample determined by EDS.

Element	Zn	O	Co	S	Ni
At%	10.88	59.57	10.95	12.52	6.07

Table S2 Comparison of specific capacitance of ZnO NFAs/CoS NFs composite in this study with other previously reported Zn-based and Co-based electrode materials for supercapacitors.

Electrode materials	Electrolyte	Current density (A g^{-1})	Specific capacitance (F g^{-1})	Ref.
ZnO NFAs/CoS NFs	**2 M KOH**	**1**	**1416**	**This work**
		15	**954**	
ZnO/NiS/CNT	3 M KOH	1.5	879	4
ZnO nanomembranes	6 M KOH	1	846	5
ZnO/N-OHPC	6 M KOH	1	720	6
Zn-doped $NiCo_2O_4$	6 M KOH	2	1344	7
ZnCoS	2 M KOH	1	1134.7	8
ZnCoO-G	2 M KOH	1	711.6	9
NiS@CoS	2 M KOH	1	1210	10
$ZnMn_2O_4$ nanosheets	0.5 M Na_2SO_4	1	456.8	11
Zn-Co-Se	1 M KOH	0.5	522.4	12
Co_3O_4@Ni-Co LDH	2 M KOH	0.5	1318	13

Ni_2CoHCF/NF	2 M KOH	0.5	1300	14
Ni@Co-Fe LDH nanowires	6 M KOH	1	1289	15
MnO_2/Co-HPCNFs	1 M Na_2SO_4	0.5	446	16
Ni–Co LDH/STSC	6 M KOH	1	992.2	17
Sn_1Co_4	6 M KOH	1	580.8	18
Co_9S_8@$NiCo_2O_4$ hollow nanoneedle	6 M KOH	1	1022.5	19

References

1 Y. Ouyang, X. Xia, H. Ye, L. Wang, X. Jiao, W. Lei and Q. Hao, *ACS Appl. Mater. Interfaces,* 2018, **10**, 3549−3561.

2 A. Ali, M. Ammar, Z. Yahya, M. Waqas, M. A. Jamal and E. H. M. Salhabi, *New J. Chem.*, 2019, **43**, 10583−10589.

3 X. Han, D. Zhang, Y. Qin, X. Kong, F. Zhang and X. Lei, *Chem. Eng. J.,* 2021, **403**, 126471.

4 S. S. Rao, *J. Energy Storage*, 2020, **28**, 101199.

5 F. Naeem, S. Naeem, Z. Zhao, G. Shu, J. Zhang, Y. Mei and G. Huang, *J. Power Sources*, 2020, **451**, 227740.

6 G. Wu, Y. Song, J. Wan, C. Zhang and F. Yin, *J. Alloys Compd.,* 2019, **806**, 464−470.

7 K. Gao and S. D. Li, *J. Alloys Compd.,* 2020, **832**, 154927.

8 Y. Zhang, N. Cao, S. Szunerits, A. Addad, P. Roussel and R. Boukherroub, *Chem. Eng. J.,* 2019, **374**, 347−358.

9 J. Yu, Z. Cui, X. Li, D. Chen, J. Ji, Q. Zhang, J. Sui, L. Yu and L. Dong, *J. Energy Storage,* 2020, **27**, 101165.

10 Y. Miao, X. Zhang, J. Zhan, Y. Sui, J. Qi, F. Wei, Q. Meng, Y. He, Y. Ren, Z. Zhan and Z. Sun, *Adv. Mater. Interfaces,* 2020, **7**, 1901618.

11 H. Barkhordari, H. Heydari, A. Nosrati and J. Mohammadi, *Ionics,* 2019, **25**, 275−285.

12 V. T. Chebrolu, B. Balakrishnan, D. Chinnadurai and H. J. Kim, *Adv. Mater. Technol.,* 2020, **5**, 1900873.

13 D. Han, Y. Zhao, Y. Shen, Y. Wei, L. Mao and G. Zeng, *J. Electroanal. Chem.,* 2020, **859**, 113887.

14 X. Zhu, H. Tao and M. Li, *Int. J. Hydrogen Energy,* 2020, **45**, 14452−14460.

15 S. Verma, V. Gupta, A. Khosla, S. Kumar and S. Arya, *Nanotechnology*, 2020, **31**, 245401.

16 X. Yang, W. Peng, K. Fu, L. Mao, J. Jin, S. Yang and G. Li, *Electrochim. Acta,* 2020, **340**, 135989.

17 D. Zhang, X. Guo, X. Tong, Y. Chen, M. Duan, J. Shi, C. Jiang, L. Hu, Q. Kong and J. Zhang, *J. Alloys Compd.,* 2020, **837**, 155529.

18 Y. Yu, Y. Tan, H. Zhang, B. Yang, L. Yuan, X. Shen and X. Hu, *J. Alloys Compd.,* 2020, **814**, 152199.

19 F. Zhu, W. Liu, Y. Liu and W. Shi, *Inorg. Chem. Front.,* 2019, **6**, 982−987.